AIAA JOURNAL
Vol. 36, No. 2, February 1998

Quantification of Mixing and Mixing Rate from Experimental Observations

R. Everson,* D. Manin,† and L. Sirovich‡
Rockefeller University, New York, New York 10021
and
M. Winter§
United Technologies Research Center, East Hartford, Connecticut 06108

A new measure of mixedness, based on entropy considerations, and a related mixing rate are introduced. It is argued that the time rate of change of the mixedness is proportional to the mixing rate. The new measures are applied to experimental observations on an axisymmetric jet and an array of jets in crossflow. The concentration field of an axisymmetric jet is measured at 10 downstream locations by optical imaging of Rayleigh scattering from a laser sheet. Mixedness and mixing rate are calculated for each of the locations. In agreement with theory, the mixedness of the self-similar jet is constant along the length of the jet. The measures allow us to locate the instantaneous realization that is most typical in terms of mixedness and mixing rate. Also analyzed is the mixing of a row of jets injecting fluid into a crossflow. The jets are sufficiently close that there is significant interaction between neighboring jets. The mixedness and mixing rate were calculated. Well-mixed regions have a low mixing rate, whereas poorly mixed regions tend to mix most rapidly. The mixedness and mixing rate allow the assessment of the effectiveness of different orifice shapes in promoting rapid mixing.

Introduction

MIXING processes play a vital role in the operation of combustors for air-breathing propulsion systems. This paper is concerned primarily with the nature of these mixing processes and how they can be assessed in quantitative terms from data acquired using advanced laser imaging techniques. A longer-range goal of this research is to develop methods and criteria for the management and prediction of the mixing process. A measure of mixedness based on configurational entropy is introduced and related to the mixing rate. The measures are applied to the mixing of an axisymmetric jet and to an array of jets in crossflow that model a specific gas turbine combustor problem. The methodology is applicable to virtually every aspect of technology and engineering in which mixing processes are important.

An example of a mixing-dominated problem is the gas turbine combustor. The design and performance of a gas turbine combustor requires good mixing characteristics to achieve high burning rates, low soot and oxides of nitrogen (NO_x) formation, and exhaust temperature uniformity. Typically, however, complete mixing can be accomplished only at the expense of combustor length and pressure loss. A gas turbine combustor flow path is characterized by three distinct zones: a primary zone, in which combustion occurs; an intermediate zone, in which mixing-driven species recombination (to lower gas temperatures) occurs; and a dilution zone, in which coolant air is injected and mixed with the combustion gases to achieve a desired turbine inlet temperature. Specific geometries[1] to achieve low NO_x emissions for the High-Speed Civil Transport rely on fast mixing either before injection to the combustor or in a quench zone downstream of a rich combustion zone. Current designs for these dilution or quench zones resort to a series of round jets, or other geometric shapes, injecting cold air at right angles to the primary gas flow to achieve the highest degree of mixing. The rich-burn/quick-mix/lean-burn (RQL) combustor uses axially staged burning zones to avoid stoichiometric mixtures in order to minimize NO_x production, while maintaining a high level of combustor efficiency. The quick-mix section is a key technology in order for this combustor to achieve low emissions. The rate of mixing, however, is strongly influenced by the hole shape, momentum ratio of the jet/primary flow, turbulence level, axial distance, etc.

To date, mixing optimization has been largely an empirical process, and any assessment of induced mixing has been indirectly inferred. Efficient design of such machines requires quantitative information about the degree and rate of mixing attained for different configurations. Laser diagnostic techniques, including Lorentz/Mie,[2] Rayleigh[3] and Raman[4] scattering, and planar laser-induced fluorescence,[5–8] allow quantitative measurements of the concentration field at single instants in time. Although these techniques continue to mature and begin to be used in the design of combustion systems, adequate means of ascertaining quantitative measures of mixing from these data still need to be addressed.

Perhaps the coarsest and most widespread measure of a passive scalar field is the rms value of fluctuations of concentration about the mean:

$$\langle [\rho(\boldsymbol{x}) - \langle \rho(\boldsymbol{x}) \rangle]^2 \rangle^{\frac{1}{2}} \tag{1}$$

where $\rho(\boldsymbol{x})$ denotes the concentration of the passive scalar at $\boldsymbol{x}$ and angle brackets denote the ensemble average. The smaller the average rms fluctuation, the better mixed is the flow. However, although Eq. (1) furnishes us with information that locates and measures the fluctuations, it does not address the scales of the fluctuations or the rate at which mixing occurs. Dahm and Dimotakis[9] have examined mixing and entrainment in turbulent jets, paying particular attention to the large-scale, organized motions. Winter et al.[10] have examined other mixing measures.

We advance new measures of mixedness and mixing rate and apply them to experiments. The first experiment examines the relatively simple axisymmetric jet. The second models the quench zone of a gas turbine combustor and consists of a pair of directly opposed rows of jets injecting fluid into a crossflow. In the following section, we describe the experimental arrangements. The measures of mixing and mixing rate then are introduced, after which we discuss the results of applying them to the experimental data. Although the data that are analyzed are from a physical experiment, the methodology is applicable generally and could just as easily have been applied to a computationally generated database.

Received April 4, 1995; revision received June 30, 1997; accepted for publication July 19, 1997.

*Assistant Professor; currently Research Associate, Department of Electrical and Electronic Engineering, Imperial College of Science, Technology, and Medicine, Exhibition Road, London SW7 2BT, England, United Kingdom. E-mail: reverson@ic.ac.uk.
†Postdoctoral Research Associate.
‡Visiting Professor.
§Manager, Advanced Optical Diagnostics. Member AIAA.

Description of Experiments

Axisymmetric Jet

In the first experiment, an axisymmetric jet, equipped with a coflow, was used to flow propane through a central orifice of diameter 4 mm. The Reynolds number based on the orifice diameter was 8×10^3. The flow was intersected at 1, 2, . . . , 10 diameters downstream by a sheet of 532-nm laser light produced by a Nd:YAG laser. The Rayleigh-scattered light was recorded on an unintensified, thermoelectrically cooled charge-coupled device (CCD) camera. The purpose of the coflow (velocity 5 cm/s) was to prevent extraneous dust from entering the imaged region. After correction for background and optical response, images were obtained in which the intensity was proportional to the flowfield concentration. Typical images from 2, 4, 6, and 8 diameters downstream are shown in Fig. 1. We remark that instantaneous profiles are top-hat shaped, rather than smoothly decaying like the mean profile (not shown). This observation is in agreement with that of Dahm and Dimotakis[9]: It implies that unmixed fluid is entrained deep into the jet and suggests that the jet is poorly characterized by the mean profile.

RQL Model

The second experiment was directed toward subsonic jets in confined crossflow. Such problems previously have been studied experimentally by Vranos and Liscinsky.[11] In their experiment, advanced data acquisition techniques using optically based diagnostics[12] furnish us with a wealth of detailed and highly resolved data. Figure 2 is a schematic representation of the apparatus, which consisted of three parallel contiguous ducts of rectangular cross section, simulating a sector of an annular combustor. Sector width was 305 mm and the inner duct height was set at 50.8 mm for the reported experiments. The outer ducts (shrouds), which supply the injectant gas, were 25 mm in height. These are separated from the inner duct by removable, 3-mm-thick flat plates. The injectant was fed from the shrouds to the inner duct through orifices of various sizes and shapes machined into the plates. Jet fluid was injected from the upper and the lower walls through orifices consisting of either round holes or slanted slots (see Fig. 2). Mass flow to each of the three ducts was controlled independently using venturi flowmeters. The maximum variation in the mean approach velocity of the mainstream flow was 6% with a turbulence level of 1.3%. Air was both the injectant and central duct fluid, so that the density ratio was one.

Planar digital imaging was used to optically measure concentration distributions in planes perpendicular to the duct axis, starting at the leading edge of the orifice and continuing downstream to a location equal to the duct height. The Mie scattering technique[5] was used by marking the jet flow with an oil aerosol of submicron-sized particles. A light sheet (0.5-mm thick) was created using a 2-W argon–ion laser and a rotating mirror. The flowfield was illuminated by passing the light sheet through a window in the side wall of the test section. An image-intensified thermoelectrically cooled CCD camera (Photometrics Star 1), located inside the duct 0.76 m downstream of the orifice centerline, was focused on the illuminated plane to provide an end-on view. The camera was synchronized to make instantaneous exposures coincident with the sweep of the beam through the flowfield. The image was digitized and sent to a computer for storage. (The data acquisition scheme is described in detail by Liscinsky et al.[12]) After correction for background and response, the scattered-light intensity was proportional to the number of particles in the

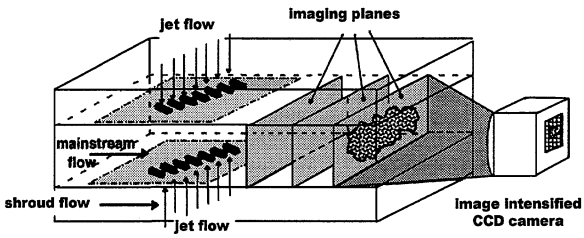

Fig. 2 Schematic diagram of RQL model experiment.

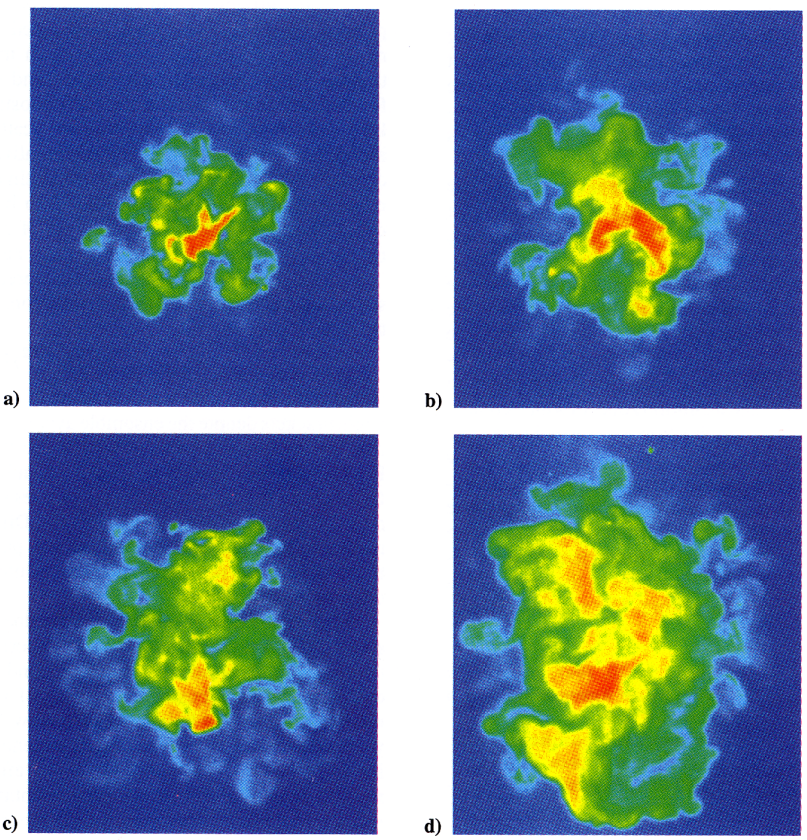

Fig. 1 Typical snapshots of concentration field from an axisymmetric jet downstream from the orifice at a) 2, b) 4, c) 6, and d) 8 diameters.

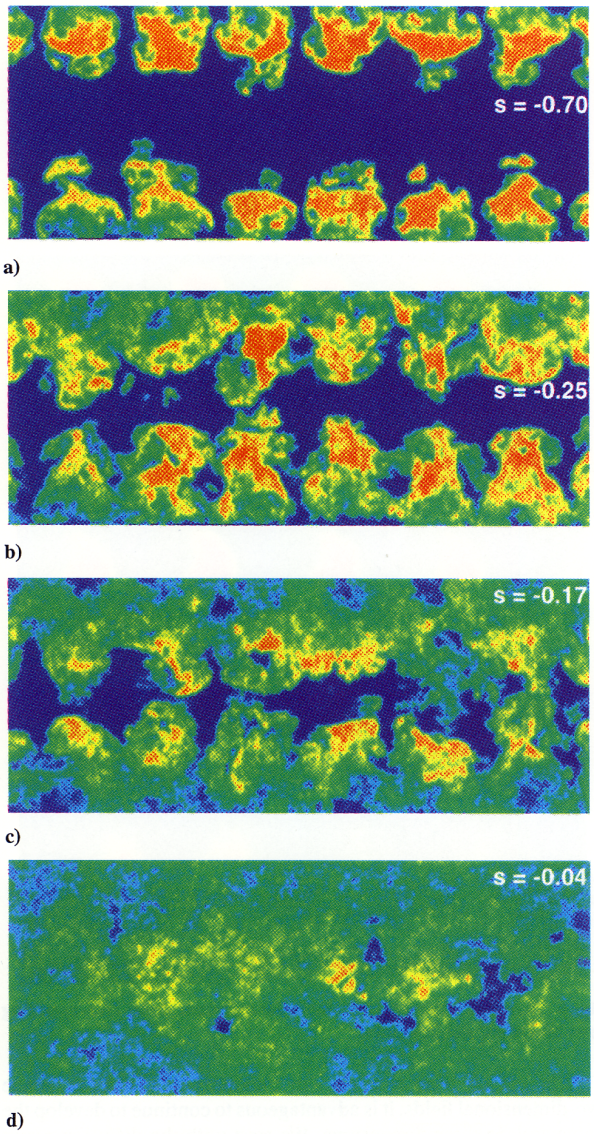

Fig. 3 Typical snapshots of concentration field downstream from two opposing rows of circular injectors. Fluid is injected vertically from the top and the bottom of the pictures, and the crossflow is directed out of the picture. Each snapshot is labeled with its entropy s that measures its mixedness, as discussed in the text. Snapshots are at a) 0.87, b) 1.28, c) 1.88, and d) 4.26 diameters downstream of the center of the orifices.

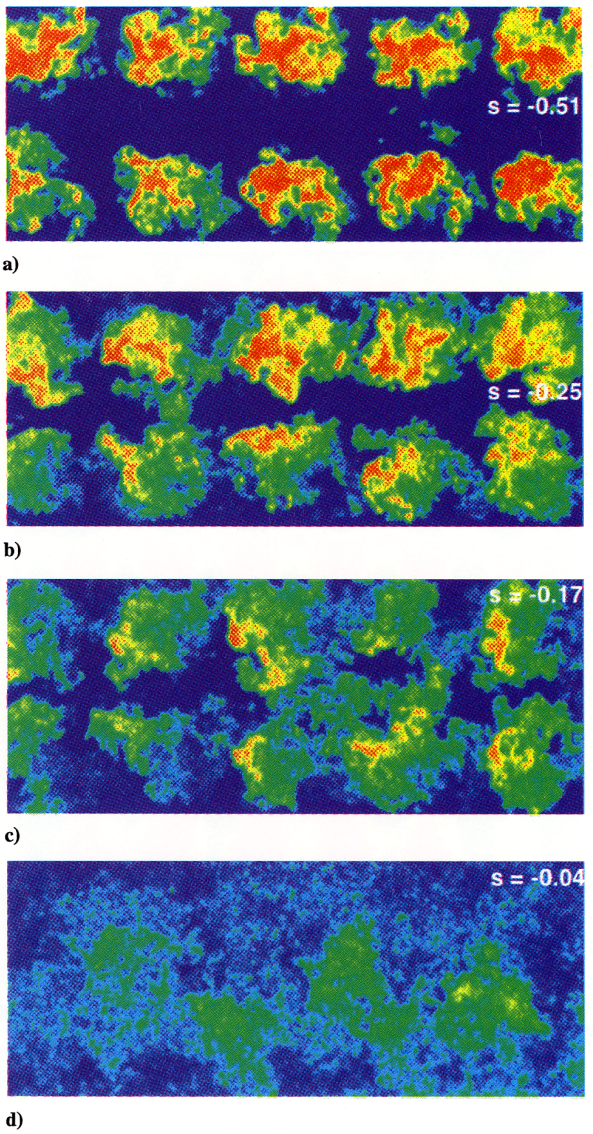

Fig. 4 Typical snapshots of concentration field downstream from two opposing rows of slanted slot injectors. Measured in units of the diameter of a circular orifice with the same diameter, the snapshots are at downstream of the center of the orifices at a) 0.63, b) 1.0, c) 1.64, and d) 4.00 diameters.

measurement volume. If only one of two streams is marked (in this study, the jet fluid), the light intensity of the undiluted marked fluid represents mole fraction unity. Instantaneous realizations of the mole fractions at four different downstream locations are shown in Figs. 3 and 4 for round holes and slanted slots, respectively. In Figs. 3 and 4, fluid is injected vertically from orifices at the top and bottom edges of the picture into a crossflow out of the page. One hundred realizations, each in a 576 × 388 format with 10-bit resolution, were recorded at each downstream location for each of the two injectors. Average concentration fields are shown in Figs. 5 and 6. Here, too, the smoothly decaying average concentrations are poor representatives of the instantaneous concentration profiles produced as unmixed ambient fluid is entrained close to the cores of the jets.

Mixedness and Mixing Rate

In this section, we introduce a new measure of mixedness, based on entropy, and relate it to the rate of mixing in the fluid. The basic approach follows arguments given in statistical mechanics.[13] We mention in passing that Pope[14] has used an entropy principle to obtain probability distribution functions in related flows. We proceed generally and partition the concentration field $\rho(\boldsymbol{x})$ into a grid of cells, for the present ρ represents the concentration in three dimensions. If the mixing species is comprised of n identical molecules, we denote the number of molecules in the lth cell as n_l, so that if the cell centered at $\boldsymbol{x}_l$ has volume $\delta\boldsymbol{x}$,

$$\rho(\boldsymbol{x}_l)\delta\boldsymbol{x} \approx n_l \tag{2}$$

and

$$\sum_l n_l = n \tag{3}$$

The measured concentration distribution can be achieved by

$$\frac{n!}{n_1!n_2!\ldots n_l!} \tag{4}$$

arrangements of the molecules (not counting arrangements that are indistinguishable). When the fluid is poorly mixed so that the molecules are concentrated in just a few cells, the number of distinct arrangements is small compared with that in a uniformly mixed fluid, in which there are the same number of molecules in each cell. The configurational entropy of the distribution is

$$S = \ell_n \frac{n!}{\prod_l n_l!} = \ell_n n! - \sum_l \ell_n n_l! \tag{5}$$

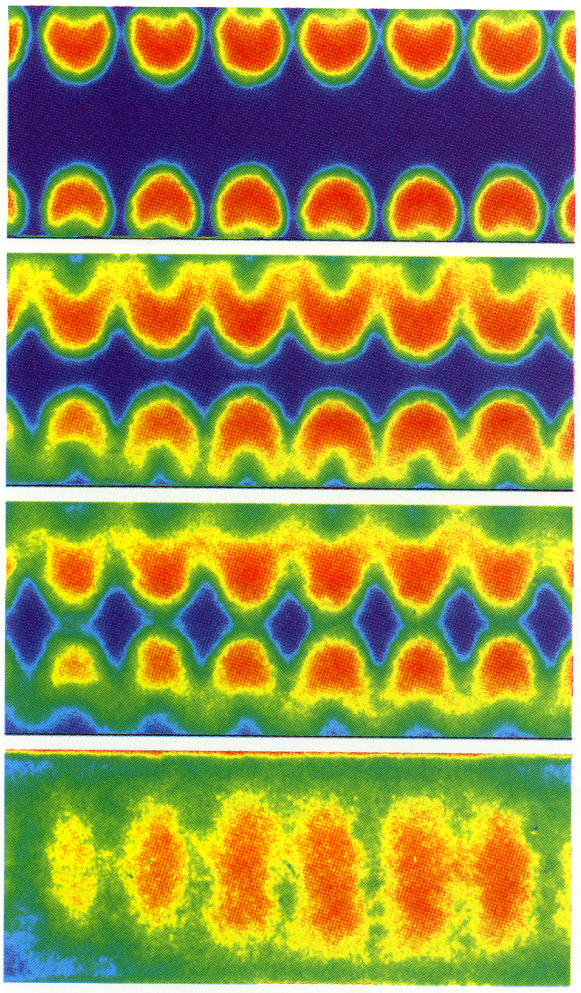

Fig. 5 Average concentration field downstream from two opposing rows of circular injectors.

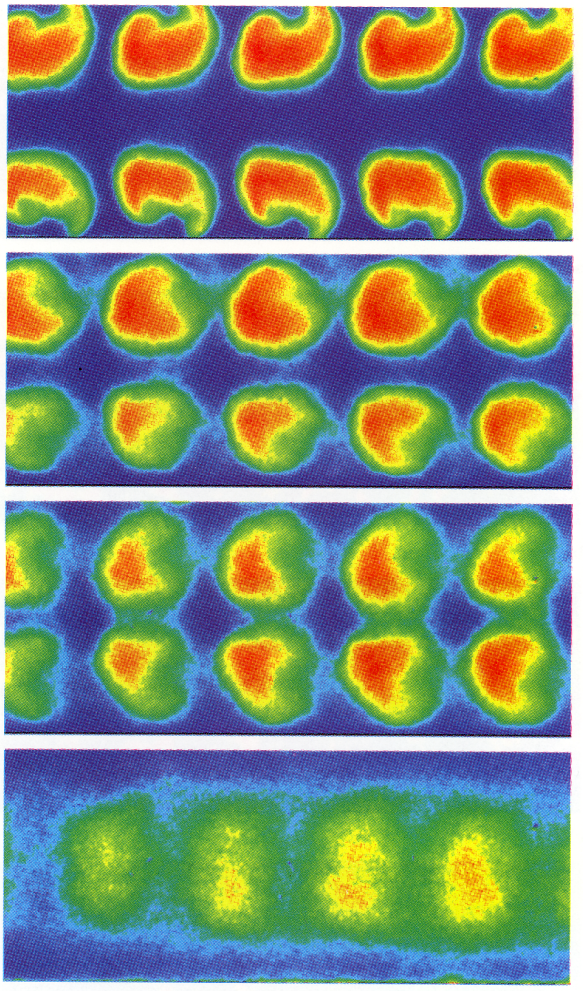

Fig. 6 Average concentration field downstream from two opposing rows of slanted slot injectors.

If we use Stirling's approximation, i.e., $\ell n m! \approx m \ell n m - m$, we obtain

$$S \approx n \ell n n - \sum_l n_l \ell n n_l \tag{6}$$

When the number of scatters in each image plane is constant, we can drop $n \ell n n$ and write

$$S = -\sum_l n_l \ell n n_l \tag{7}$$

Next, we consider entropy per unit density, $s = S/\rho_0$, where ρ_0 is a reference value. Then, up to a constant (provided that the number of scatters in the image plane is constant), s is given by

$$s = -\int \frac{\rho}{\rho_0} \ell n \frac{\rho}{\rho_0} \, d\boldsymbol{x} = -\int \sigma \ell n \sigma \, d\boldsymbol{x} \tag{8}$$

where $\sigma = \rho/\rho_0$.

Figure 7 exhibits the entropy for four different snapshots. These data are Mie scattering images collected downstream of two rows of round holes injecting fluid. The entropy clearly agrees with the intuitive notion of mixedness: The panels with high entropy are better mixed than those with low entropy. Note that all four panels come from a single flow condition. The wide variation in mixedness makes visual assessment of the average degree of mixing difficult. The average entropy, however, characterizes the mean mixedness.

Also shown is the rms concentration fluctuation, $[\int (\rho - \rho_0)^2 \, d\boldsymbol{x}]^{1/2}$, for each frame. The entropy distinguishes between the middle frames, which have the same rms fluctuation. We point out that, when the fluctuations are small, so that $\rho(\boldsymbol{x}) \approx \rho_0[1 + \epsilon \rho'(\boldsymbol{x})]$ and $\int \rho'(\boldsymbol{x}) \, d\boldsymbol{x} = 0$, the entropy is well approximated by the rms fluctuation divided by the mean concentration.

Although we wish to apply our measures to snapshots, hence two-dimensional fields, it is advantageous to continue to develop the framework in three dimensions. We start with the diffusion equation

$$\frac{\partial \sigma}{\partial t} + \nabla \cdot (\sigma \boldsymbol{u}) = \kappa \nabla^2 \sigma \tag{9}$$

which governs mixing. The (turbulent) flow $\boldsymbol{u}$ is taken to be incompressible, $\nabla \cdot \boldsymbol{u} = 0$. Data analysis of concentration fields is based on averages over many images, and thus among other reasons, we should consider ensemble averages. This is denoted by angle brackets or bars, e.g.,

$$\langle \boldsymbol{u} \rangle = \bar{\boldsymbol{u}} \tag{10}$$

If we write

$$\boldsymbol{u} = \bar{\boldsymbol{u}} + \boldsymbol{u}' \tag{11}$$

then it follows that

$$\nabla \cdot \bar{\boldsymbol{u}} = 0 = \nabla \cdot \boldsymbol{u}' \tag{12}$$

If Eq. (11) is substituted into Eq. (9) and an ensemble average is performed, we obtain

$$\frac{\partial \bar{\sigma}}{\partial t} + \nabla \cdot (\bar{\sigma} \bar{\boldsymbol{u}}) + \nabla \cdot (\overline{\sigma \boldsymbol{u}'}) = \kappa \nabla^2 \bar{\sigma} \tag{13}$$

For conceptual purposes it is convenient to replace the turbulent mixing $\overline{\sigma \boldsymbol{u}'}$ with an eddy diffusivity κ_e; hence

$$\overline{\sigma \boldsymbol{u}'} = -\kappa_e \nabla \bar{\sigma} \tag{14}$$

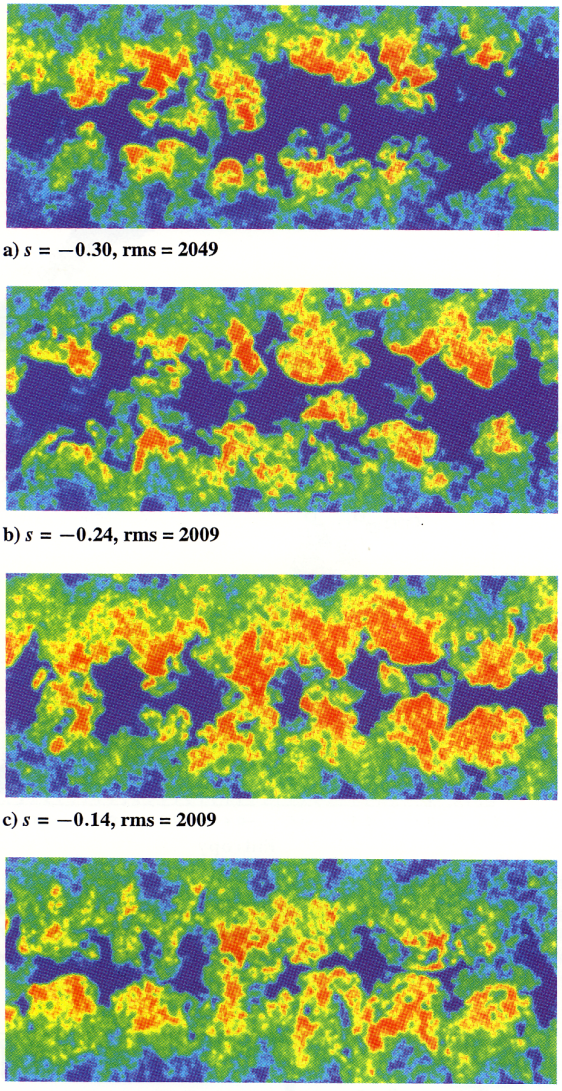

a) $s = -0.30$, rms = 2049

b) $s = -0.24$, rms = 2009

c) $s = -0.14$, rms = 2009

d) $s = -0.09$, rms = 2009

Fig. 7 Entrophy as a measure of mixedness. The four snapshots, all from the same station under the same flow conditions, are marked with the entrophy s that measures the mixedness of the snapshot.

Thus, Eq. (13) becomes

$$\frac{\partial \bar{\sigma}}{\partial t} + \nabla \cdot (\bar{\sigma}\bar{\boldsymbol{u}}) = \nabla \cdot [(\kappa + \kappa_e)\nabla\bar{\sigma}] \tag{15}$$

We introduce

$$h = -\int \bar{\sigma}\, \ell n \bar{\sigma}\, \mathrm{d}\boldsymbol{x} \tag{16}$$

which, in the present framework, is the counterpart of H in Boltzmann's H-theorem.[15] From this, it follows that

$$-\frac{\mathrm{d}h}{\mathrm{d}t} = -\int (1 + \ell n \bar{\sigma}) \frac{\partial \bar{\sigma}}{\partial t}\, \mathrm{d}\boldsymbol{x} \tag{17}$$

$$= \int \nabla \cdot [\bar{\boldsymbol{u}}\bar{\sigma}\, \ell n \bar{\sigma} - (\kappa + \kappa_e)\nabla\bar{\sigma}]\, \mathrm{d}\boldsymbol{x}$$

$$- \int (\kappa + \kappa_e) \frac{(\nabla\bar{\sigma})^2}{\bar{\sigma}}\, \mathrm{d}\boldsymbol{x} \tag{18}$$

Because $\bar{\boldsymbol{u}} \cdot \boldsymbol{n} = \boldsymbol{n} \cdot \nabla\bar{\sigma} = 0$ on the boundaries of the domain, it follows that

$$\frac{\mathrm{d}h}{\mathrm{d}t} = 4 \int (\kappa + \kappa_e) \left(\nabla \bar{\sigma}^{\frac{1}{2}}\right)^2 \mathrm{d}\boldsymbol{x} \tag{19}$$

Because h measures the mixedness, we call the quantity

$$R = \int \left(\nabla \bar{\sigma}^{\frac{1}{2}}\right)^2 \mathrm{d}\boldsymbol{x} \tag{20}$$

the rate of mixing. A similar quantity for measuring mixing appears in Ref. 10.

To relate these considerations to two-dimensional concentration fields, we focus for the moment, on the case of our axisymmetric jet. We denote the streamwise variable by z and integrate Eq. (17) into the transverse plane:

$$-\frac{\partial}{\partial t} h_2(z, t) = -\frac{\partial}{\partial t} \int \bar{\sigma}\, \ell n \bar{\sigma}\, \mathrm{d}x\, \mathrm{d}y$$

$$= \int \left[\frac{\partial}{\partial z}(\bar{u}_z \bar{\sigma}\, \ell n \bar{\sigma}) + \nabla_2 \cdot (\bar{u}_2 \bar{\sigma}\, \ell n \bar{\sigma})\right] \mathrm{d}x\, \mathrm{d}y$$

$$- \int (1 + \ell n \bar{\sigma}) \nabla \cdot [(\kappa + \kappa_e)\nabla\bar{\sigma}]\, \mathrm{d}x\, \mathrm{d}y \tag{21}$$

Here, $\bar{\boldsymbol{u}}_2 = (\bar{u}_x, \bar{u}_y)$ and $\nabla_2 = [(\partial/\partial x), (\partial/\partial y)]$.

To proceed further, we adopt the reasonable assumption that streamwise derivatives are small compared with transverse derivatives, so that $\nabla \cdot [(\kappa + \kappa_e)\nabla\bar{\sigma}] \approx \nabla_2[(\kappa + \kappa_e)\nabla_2\bar{\sigma}]$. On introducing this into Eq. (21) and proceeding as in Eq. (20), we obtain

$$\frac{\partial h_2}{\partial t} + \frac{\partial}{\partial z}(U h_2) = 4 \int (\kappa + \kappa_e) \left(\nabla_2 \bar{\sigma}^{\frac{1}{2}}\right)^2 \mathrm{d}x\, \mathrm{d}y \tag{22}$$

U is a suitably defined streamwise velocity, e.g., the centerline mean velocity yields a good approximation.

The development just presented furnishes a guide for more general jet flows, viz., we can regard z as the curvilinear distance along the jet centerline and (x, y) as the transverse directions. The jet in crossflow is representative of a more general flow. For technical reasons, it was not possible to acquire images in planes perpendicular to the flow direction, which somewhat compromises the results given later, because the number of scatterers in image planes at different stations may be different, which means that the term $n\, \ell n n$ in Eq. (6) cannot be neglected. However, the mean flux at each station (as measured by the mean scattered light) is approximately constant and the analysis has, at least, a comparative value.

Although this theoretical analysis has considered the entropy of ensemble averages of the concentration, it is also of interest to examine the distribution of the entropies of individual snapshots of the flowfield. To this end, an entropy and mixing rate can be calculated for each snapshot. (Again, care must be exercised if the image planes are not normal to the mean flow.) This view furnishes information on the fluctuations in mixedness at a particular station. We remark that, because individual snapshots generally are not as smooth as the ensemble average, their entropies are more negative than the entropy of the ensemble average.

Results

Axisymmetric Jet

Entropies s and mixing rates R were calculated for instantaneous concentration fields of the axisymmetric jet at $z = 1, 2, \ldots, 10$ diameters downstream of the orifice. Unlike the combustor experiment, the jet is not confined to a fixed cross-sectional area but expands in a self-similar manner so that its radius $r(z)$ is proportional to the downstream distance z. [Defining $r(z) = (\int \rho r^2\, \mathrm{d}r)/(\int \rho r\, \mathrm{d}r)$, this was experimentally verified for the jet described here, when $z > 3$ diameters.] Although the jet is not fully self-similar in the region $3 < z < 10$, i.e., the velocity profiles are not yet self-similar, it is sufficiently far from the orifice for only one length scale, the distance from the orifice, to be relevant. There is no dimensionless combination involving z, other than a constant, on which the entropy (a dimensionless quantity) may depend. Sufficiently far downstream, therefore, we can expect the entropy to be constant, provided that an appropriate domain for calculating s is chosen. The correct domain should be consistent with the self-similar expansion of the jet; that is, it should be calculated in a domain that grows in proportion to the jet radius. This choice of domain also ensures that the

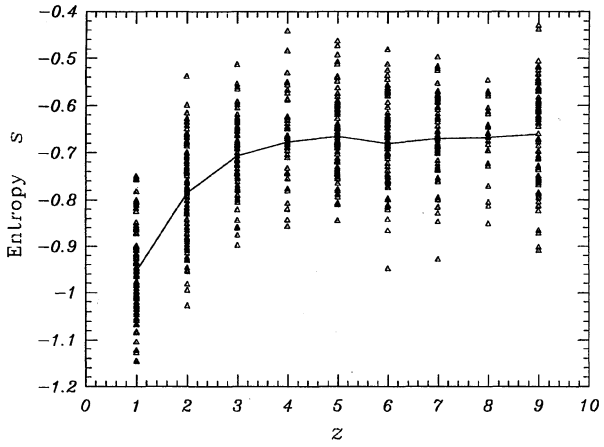

Fig. 8 Entropy in the axisymmetric jet as a function of distance from the orifice. Each symbol represents an individual measurement, and the line joins the average entropies at each measurement station. Entropy is calculated over a domain that is normalized to the jet diameter.

number of scatterers in each image plane is constant, permitting the approximation made in Eq. (6).

Figure 8 shows entropy at each of the longitudinal stations, calculated for circular domains embracing the jets, with radii proportional to the local jet radius. The average of the instantaneous entropies at each station also is shown. The calculated entropy is consistent with the scaling expected from the self-similar expansion of the jet. The departures at the first two stations can be attributed to the still-developing, undermixed flow close to the orifice and to residual out-of-focus images of the orifice itself, which are prominent in images recorded at the first station and visible in those recorded at the second.

RQL Model

The entropy and mixing rate have been calculated for ensembles of concentrations measured downstream of two rows of orifices modeling the injector configuration in a gas turbine combustor. Figure 9 shows the mixing rate R plotted against the entropy s. Each individual symbol corresponds to a particular snapshot, and different symbols denote different locations and orifice shapes (diagonal slots or holes). At locations closest to the orifices, the entropy and the mixing rates are high, indicating a poorly mixed flow that is mixing rapidly. Farther away from the orifices, the flow is better mixed, and the rate of mixing has declined. There is clearly considerable scatter in both the entropy and the mixing rate at each location, but the average quantities lie on a well-defined locus.

Figure 10 compares the entropy as a function of downstream distance for the mixing flows generated by circular and slanted slot orifices. The area of the slots was equal to the area of the circular holes. Distances are measured from the center of the rows of orifices, and are stated in units of the circular hole diameter. Consequently, the leading and trailing edges of the slots extend farther up- and downstream than the circular holes. This means that the slots begin mixing before the holes, which is reflected by the lower entropy (better mixed) for the slots at less than one diameter downstream. Farther downstream, the flows generated by the slots and holes can be said to be equally mixed, and little advantage is to be gained by using one or the other orifice shape. It is to be expected, however, that different orifice shapes will enhance or deplete the rate of mixing in flows in which the momentum of the injected fluid is less.

Note that the image planes were not normal to the mean flow direction, which bends as the injected fluid is entrained into the main flow. Consequently, the assumption that the number of scatterers in each image plane is constant may not be warranted. Technical limitations precluded making the image planes normal to the mean-flow direction and, in any case, it is of interest in engineering applications to assess the degree of mixedness at specific distances from the orifices. This means that our theoretical development cannot be applied without some caution; nonetheless, the entropies of the snapshots at

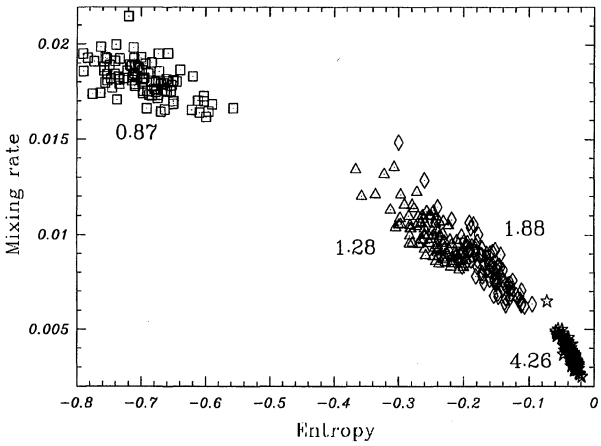

a) Circular orifices

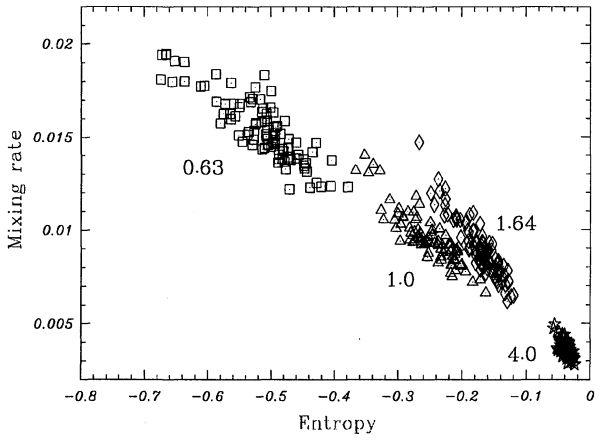

b) Slanted-slot orifices

Fig. 9 Mixing rate R plotted against entropy s. Each symbol represents an individual snapshot. Measurement stations are designated by symbols shapes, and the downstream location is indicated by the numbers by each cluster.

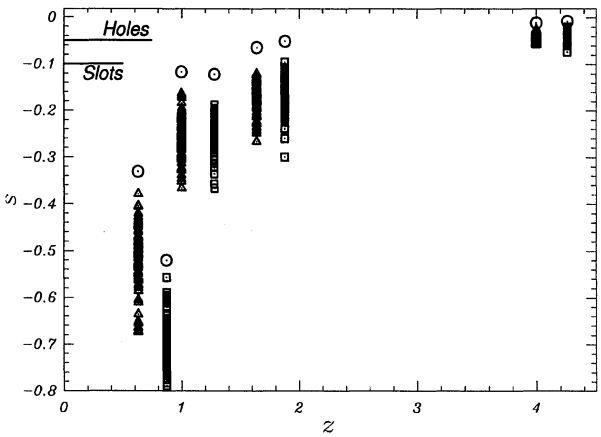

Fig. 10 Entropy s plotted against downstream distance for circular (□) and slanted-slot (△) orifices. Each symbol represents an individual measurement. Also plotted is the entropy h at each station (○). Distances are measured from the center of the rows of orifices, and the downstream extent of the orifices is indicated by the horizontal lines.

the various locations permit comparisons of the efficacy of different orifices.

Also, we note the important difference between s [Eq. (8)] and h [Eq. (16)]. Without ensemble averaging, we obtain an almost reversible process, in which the relatively small molecular diffusion κ accounts for irreversibility; s is the appropriate entropy in this case. With the introduction of averaging, the much larger eddy diffusivity κ_e appears [Eq. (14)] and h is the appropriate entropy. Both values of entropy are shown in Fig. 10.

Plots such as Fig. 9 allow us to locate the most typical snapshot in terms of mixedness and mixing rate: That is, the snapshot with coordinates (s_i, R_i) closest on the graph to the mean $(\langle s \rangle, \langle R \rangle)$. In fact, the typical snapshots shown in Figs. 3 and 4 were selected in exactly this manner. These typical snapshots are clearly quite different from the mean concentration fields $\bar{\rho}(\boldsymbol{x})$, in which only large scales survive, and are impossible to locate without an objective measure of mixing.

Summary and Conclusions

This paper focuses on the quantification of mixing and mixing rate. We introduce new measures: the mixedness or entropy h and the mixing rate R. In many circumstances it is expected that the following relation holds:

$$\frac{\mathrm{d}h}{\mathrm{d}t} = 4 \int (\kappa + \kappa_e)\left(\nabla \tilde{\sigma}^{\frac{1}{2}}\right)^2 \mathrm{d}\boldsymbol{x} \tag{23}$$

Entropies are calculated for instantaneous cross-sectional measurements of a self-similar axisymmetric jet and the mean entropy is found to be constant along the jet, in agreement with scaling arguments.

The entropy and mixing rate are calculated for ensembles of concentrations collected at different locations in an experimental model of a gas combustor quench region. The wide variation in mixedness at any single station makes visual assessment of the degree of mixing difficult. The average entropy and mixing rate characterize the flows and provide objective criteria to allow optimization of the orifice shape to promote rapid mixing.

Acknowledgments

This work was supported by NASA Contract NAS3-25954, Task Order 12, from NASA Lewis Research Center and by United Technologies Corporation. We are grateful to David Liscinsky for providing us with the slot and hole data. We also would like to express our thanks to J. D. Holdeman of NASA Lewis Research Center for many useful discussions and for his support of this work. Thanks for many helpful comments also is due to the reviewers.

References

[1]Shaw, R. J., "Engine Technology Challenges for a 21st Century High Speed Civil Transport," NASA TM 104363, 1991.

[2]Long, M., Chu, B., and Chang, R., "Instantaneous Two-Dimensional Gas Concentration Measurements by Light Scattering," *AIAA Journal*, Vol. 19, No. 9, 1981, pp. 1151–1157.

[3]Escoda, M., and Long, M., "Rayleigh Scattering Measurements of the Gas Concentration Field in Turbulent Jets," *AIAA Journal*, Vol. 21, No. 1, 1983, pp. 81–84.

[4]Long, M., Fourguette, D., Escoda, M., and Lane, C., "Instantaneous Ramanography of a Turbulent Diffusion Flame," *Optics Letters*, Vol. 8, No. 5, 1983, pp. 244–246.

[5]Dyer, M., and Crosley, D., "Two-Dimensional Imaging of OH Laser-Induced Fluorescence in a Flame," *Optics Letters*, Vol. 7, No. 8, 1982, pp. 382–384.

[6]Lozano, A., Yip, B., and Hanson, R., "Acetone: A Tracer for Concentration Measurements in Gaseous Flows by Planar Laser-Induced Fluorescence," *Experiments in Fluids*, Vol. 13, 1992, pp. 369–376.

[7]Yip, B., Lozano, A., and Hanson, R., "Gas Phase Molecular Mixing Measurements Using the Acetone–Biacetyl System," AIAA Paper 93-0221, Jan. 1993.

[8]Winter, M., Hermanson, J., and Dobbs, G., "Imaging of Molecular Mixing in a Gas-Phase Turbulent Jet by Collisional Energy-Transfer Fluorescence," AIAA Paper 92-0381, Jan. 1992.

[9]Dahm, W., and Dimotakis, P., "Measurement of Entrainment and Mixing in Turbulent Jets," *AIAA Journal*, Vol. 25, No. 9, 1987, pp. 1216–1223.

[10]Winter, M., Barber, T., Everson, R., and Sirovich, L., "Eigenfunction Analysis of Turbulent Mixing Phenomena," *AIAA Journal*, Vol. 20, No. 7, 1992, pp. 1681–1688.

[11]Vranos, A., and Liscinsky, D., "Planar Imaging of Jet Mixing in Crossflow," *AIAA Journal*, Vol. 26, No. 11, 1988, pp. 1297, 1298.

[12]Liscinsky, D., True, B., and Holderman, J., "Mixing Characteristics of Directly Opposed Rows of Jets Injected Normal to a Crossflow in a Rectangular Duct," AIAA Paper 94-0217, Jan. 1994.

[13]Schrodinger, E., *Statistical Thermodynamics*, Cambridge Univ. Press, Cambridge, England, UK, 1946.

[14]Pope, S., "Probability Distributions of Scalars in Turbulent Shear Flow," *Turbulent Shear Flows*, edited by J. Bradbury, F. Durst, F. Schmidt, and J. Whitelaw, Vol. 2, MIT Press, Cambridge, MA, 1979, pp. 7–16.

[15]Chapman, S., and Cowling, T., *The Mathematical Theory of Non-Uniform Gases*, Cambridge Univ. Press, New York, 1939.

F. W. Chambers
Associate Editor

Color reproduction courtesy of United Technologies Research Center